

Distribution-aware Dataset Distillation for Efficient Image Restoration

Zhuroan Zheng[†]
Sun Yat-sen University

Xin Su[†]
Fuzhou University

Chen Wu
University of Science and Technology of China

Xiuyi Jia*
Nanjing University of Science and Technology

Abstract

With the exponential increase in image data, training an image restoration model is laborious. Dataset distillation is a potential solution to this problem, yet current distillation techniques are a blank canvas in the field of image restoration. To fill this gap, we propose the Distribution-aware Dataset Distillation method (TripleD), a new framework that extends the principles of dataset distillation to image restoration. Specifically, TripleD uses a pre-trained vision Transformer to extract features from images for complexity evaluation, and the subset (the number of samples is much smaller than the original training set) is selected based on complexity. The selected subset is then fed through a lightweight CNN that fine-tunes the image distribution to align with the distribution of the original dataset at the feature level. Our method achieves promising performance on multiple image restoration tasks, including multi-task image restoration, all-in-one image restoration, and ultra-high-definition image restoration tasks. Note that we can train a state-of-the-art image restoration model on an ultra-high-definition (4K resolution) dataset using only one consumer-grade GPU in less than 8 hours (500% savings in computing resources and immeasurable training time).

1. Introduction

Image restoration provides high-quality information for downstream visual tasks such as denoising [7], deblurring [14], and deraining [41]. Recent advancements have employed deep learning techniques to boost restoration quality, achieving state-of-the-art results across various benchmarks [36, 42]. Although deep learning algorithms have shown promising results, they are highly dependent on the quantity of the datasets. Indeed, it has become a trend to create large-scale benchmarks, which unfortunately also brings

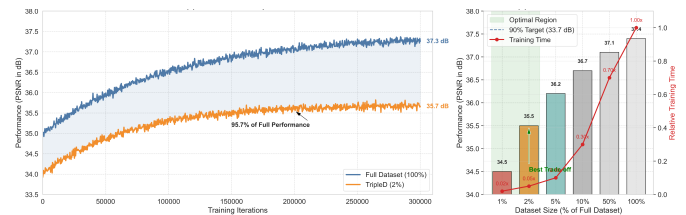


Figure 1. **Performance and analysis of our TripleD method for image restoration.** First, the figure on the left shows that using only 2% of the original dataset allows the model to perform close to training on the full set. The figure on the right demonstrates an ablation where the performance of the image restoration model rises steadily as the proportion of synthetic datasets rises, but the improvement is very limited.

expensive training costs.

To alleviate this problem, dataset distillation [32] becomes a potential option. This technique aims to synthesize a representative subset (the amount of data is much smaller than the original dataset) as a training set for the model to achieve similar performance when trained on a large-scale dataset. However, this technology is still a blank in the field of image restoration. Since the task of image restoration is a refined regression operation, there is no margin error like the classification task (for classification tasks, a probability of 0.5 to 1 indicates that the label exists).

In this paper, we design a distribution-aware dataset distillation (TripleD) algorithm, which can efficiently synthesize a small dataset from a large-scale image restoration dataset. As illustrated in Figure 1, TripleD method, which has two properties: i) A high-quality synthetic dataset can be distilled for efficient training of the image recovery model using only 2% of the data volume of the training set (PSNR reaches the upper limit of around 95%). ii) Although the model performs better as the number of synthetic datasets increases, the improvement is limited. TripleD achieves up to 90~95% of the performance of full-dataset training while utilizing only 1~5% of the data. Additionally, TripleD significantly reduces the training resource

[†]Equal contribution.

*Corresponding author: jiaxy@njjust.edu.cn.

requirements, enabling models such as Restormer to be trained efficiently on a single RTX 3090 GPU. Specifically, TripleD uses features extracted from downsampled images (the input images are all downsampled to a resolution of 128×128) using a Vision Transformer (ViT) [9] to represent the complexity of images. Here, this pre-trained Transformer is trained on the ImageNet dataset, and the label is the entropy value of the image. It is worth noting that relying only on the entropy value of the image to represent the image complexity is subject to error, and we manually conduct a significant amount of revision annotation. We use the complexity of images for key purposes: With the help of the GPU shader, Vision Transformer can be run faster on downsampled input images without losing the semantics of the original resolution image. Relying only on traditional calculations to obtain the entropy value of an image is not only time-consuming and laborious but also subject to errors. Indeed, we also considered measures such as cosine distance, standard deviation, KL divergence, and entropy, but they performed poorly in evaluating the complexity of images. For the generation of synthetic samples, we used a diffusion model, which produces better and more varied quality than GAN [8]. Finally, for distribution matching between the synthetic dataset and the selected dataset, we used a joint regularization i.e., KL scatter and L2. Our contributions are as follows:

- To the best of our knowledge, we are the first to design a dataset distillation framework (TripleD) for image restoration tasks, which alleviates the cost of training image restoration models on large-scale data sets.
- We develop an efficient dynamic distillation method that progressively increases the complexity of the sample bar to select high-quality sample clusters for distillation to obtain sub-datasets (2% of full dataset).
- Our method can also achieve dataset distillation on a single GPU in a limited amount of time when executing ultra-high-definition datasets. Extensive experimental results show that our method can help the model maintain 90% of its performance at a lower cost.

2. Related Work

Image Restoration. Image restoration aims to recover clean images from degraded inputs, addressing tasks such as denoising [40], deblurring [19], and deraining [38]. Recently, since Transformer has a strong ability to capture global features, models based on it have shown very promising results, such as Restormer [37], SwinIR [16] and IPT [6], have achieved state-of-the-art results. Unfortunately, these methods are too computationally expensive for deployment on mobile or embedded devices. So far, RAMiT [20], and FreqFormer [23], propose more efficient attention mechanisms to reduce complexity while maintaining performance. Although the inference efficiency of models

has been significantly improved, the exponential increase in data sets has not been addressed in terms of training efficiency. Dataset distillation provides a potential solution to this problem.

Subset Selection. Subset selection is a sampling technique for picking representative samples from a dataset, maintaining model performance with sampled data. Active learning [28, 29], continuous learning [18, 22], and incremental learning [26] all reduce training costs by selecting the samples with the greatest information content, such as the sample variance or entropy. For example, Settles [30] demonstrated how active learning can effectively prioritize data points, minimizing labeling efforts while maintaining high model performance. The Herding method in [3] iteratively minimizes the mean embedding discrepancy between the selected subset and the whole dataset in the feature space. Indeed, it is particularly important for image restoration tasks, which are usually high-cost due to its dense prediction. Recent advances in dynamic data selection for low-level vision tasks further highlight the need for adaptive sampling strategies that evolve during training [17, 20, 31, 34]. In this paper, we extend these principles by leveraging Vision-Language Models (VLMs) to compute selection scores, dynamically selecting samples based on complexity. This enables more efficient and targeted training, particularly in large-scale image restoration tasks.

Dataset Distillation. While dataset distillation has been successful in reducing training load for classification tasks [4, 32, 44], its application to image restoration remains challenging. The challenge is the continuous nature of outputs in image restoration, which requires precise pixel-level predictions, making it difficult to select representative samples. For classification tasks, there is some tolerance for errors. For example, a label between 0 and 0.5 may be classified as 0. In addition, image restoration involves various types of degradation, such as noise, blur, and rain, each of which introduces different complexities [38, 40]. Traditional sample selection and data synthesis methods [43] struggle to capture the full range of these degradations, leading to sub-optimal training efficiency. Recent dynamic sample selection approaches [21, 34] have begun to address these limitations, but they are still underdeveloped for tasks like image restoration, which require nuanced data selection and adaptation. In this paper, a Dynamic Data Distillation algorithm is developed to solve the problems of accurate pixel prediction and the variability of degradation types.

3. Method

In this section, we introduce the Distribution-aware Dataset Distillation (TripleD) method, which includes preliminary knowledge, image complexity calculation, and fine-tuning of data distribution (see Figure 2).

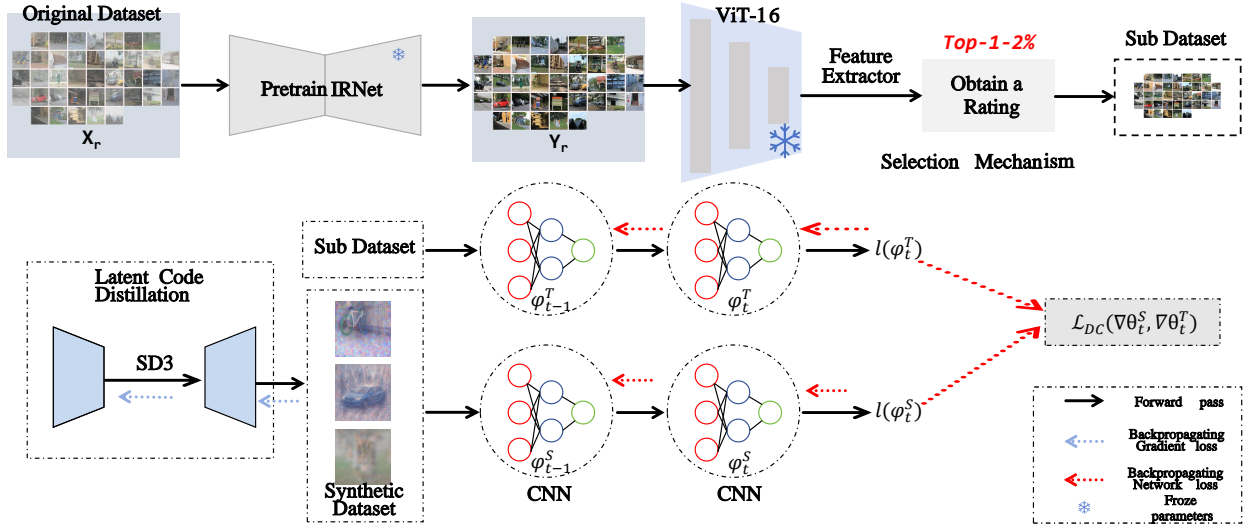


Figure 2. **Overview of the TripleD Pipeline.** A pretrained IRNet backbone (SwinIR) first processes large-scale real-degraded pairs ($X_r \rightarrow Y_r$), and a ViT-based entropy scorer selects the top 1-2% most informative samples as the real sub-dataset. Meanwhile, a diffusion-based latent distillation module (SD3) synthesizes compact training pairs whose latents match those of the selected real samples. Finally, both the distilled real and synthetic subsets are used to train the restoration network under task and distillation losses, greatly reducing training data while preserving performance.

3.1. Preliminary knowledge

Image Restoration. A trained image restoration (IR) model $\zeta_\theta : \mathbb{R}^{H \times W \times C} \rightarrow \mathbb{R}^{H \times W \times C}$ is optimized to approximate the inverse of a degradation process that maps a clear image (HQ) $y \in \mathbb{R}^{H \times W \times C}$ to its corresponding Low-Quality (LQ) counterpart $x \in \mathbb{R}^{H \times W \times C}$. The model parameters θ are optimized using a dataset $\mathcal{T} = (X_r, Y_r)$, a collection of LQ-HQ image pairs. The objective function for training the IR model is

$$\theta^* = \arg \min_{\theta} \mathbb{E}_{x_i \in X_r, y_i \in Y_r} \|\psi_\theta(x_i) - y_i\|^2. \quad (1)$$

Dataset Distillation. The goal of dataset distillation is to compress a raw dataset $\mathcal{T} = (X_r, Y_r)$, where $X_r \in \mathbb{R}^{N \times H \times W \times C}$ and N is the number of samples, into a significantly smaller synthetic dataset $\mathcal{S} = (X_s, Y_s)$ with $X_s \in \mathbb{R}^{M \times H \times W \times C}$ and $M \ll N$. In this setting, M is defined as $M = \mathcal{C} \cdot \text{IPC}$, \mathcal{C} , where \mathcal{C} is the number of classes and IPC represents the Images Per Class (IPC). The overall optimization for dataset distillation is formulated as

$$\mathcal{S}^* = \arg \min_{\mathcal{S}} \mathcal{L}(\mathcal{S}, \mathcal{T}), \quad (2)$$

where \mathcal{L} is a predefined objective for dataset distillation. It computes the loss on real data (ℓ^T) and the corresponding synthetic data (ℓ^S), then minimizes the discrepancy between the gradients of both networks:

$$\mathcal{L}_{DC} = 1 - \frac{\nabla_{\theta} \ell^S(\theta) \cdot \nabla_{\theta} \ell^T(\theta)}{\|\nabla_{\theta} \ell^S(\theta)\| \|\nabla_{\theta} \ell^T(\theta)\|}. \quad (3)$$

3.2. Selection Subset

Given a dataset \mathbf{X} , it extracts features from a pre-trained encoder (ViT-16, 16 denotes the number of layers of the model) to evaluate the complexity of the image distribution. The output of ViT comes with a Sigmoid function to squeeze the values to 0-1, and the corresponding entropy labels of the modified ImageNet dataset are also squeezed to 0-1 with the help of Max-Min normalization. Specifically, the input image is downsampled to a resolution of 128×128 by using bilinear downsampling. Here, the image is downsampled to improve the efficiency of the data distillation algorithm. Finally, we select a subset of real images in this image restoration dataset that are ranked in the top 1% or 2% of entropy values.

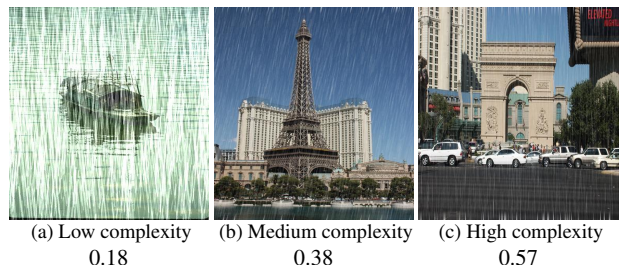


Figure 3. This figure shows the complexity of the image is evaluated by using the ViT that is pre-trained.

To better illustrate the effectiveness of this method, we visualize some degraded images to explain. Figure 3(a), featuring uniform rain streaks, exhibits the lowest variance,

indicating the simplest complexity. In contrast, Figure 3(b) shows moderate complexity, with a broader range of variance, representing a mix of simple and more varied features. Lastly, Figure 3(c), which includes diverse objects and textures, demonstrates the highest variance, reflecting the greatest complexity. It is important to note that we observe a phenomenon where the strength of the noise (rain and fog) affects the complexity of the image, and therefore, the subset selection is mainly considered on clean images. Finally, we obtain a subset dataset \mathbf{B} .

3.3. Latent Distillation for IR

In addition to pixel-level distillation, we also consider the application of Generative Latent Distillation (GLaD) [5] in the distillation of latent datasets. Instead of optimizing synthetic images directly in pixel space, GLaD operates in the latent space of the generative model (the GAN in the model, which we replace with a diffusion model (SD3)). This approach enables distillation at a higher level of abstraction, capturing complex image features while reducing the need for direct pixel-by-pixel optimization. Specifically, GLaD learns latent codes that reconstruct high-fidelity synthetic images as they pass through the generator. The method can distill large-scale image structures while preserving fine-grained details.

3.4. Data Fine-tuning via CNN

We built an 8-layer convolutional CNN network with 3×3 kernels and a step size of 1, which is used to fine-tune the distribution of the dataset \mathbf{B} (generate a latent feature space, where the features of the subset are \mathbf{F}_a and the features of the synthetic data \mathbf{B}_s are \mathbf{F}_b).

The fine-tuned dataset \mathbf{B}_s is used to train the image restoration model, and the CNN is updated with the help of the loss of the image restoration model. A simple L2 loss and KL are employed to provide pixel-level supervision:

$$\mathcal{L}_{pix} = \|\mathbf{I}_{\mathbf{F}_a} - \mathbf{I}_{\mathbf{F}_b}\|_2 + \mathcal{L}_{DC}(\mathbf{F}_a, \mathbf{F}_b), \quad (4)$$

where $\|\cdot\|_2$ denotes L2 norm, \mathcal{L}_{DC} denotes KL dispersion.

4. Experiments

In this section, we conduct extensive experiments to demonstrate the effectiveness of TripleD for image restoration tasks. Our experiment mainly contains three groups: one is multi-task image restoration, one is all-in-one image restoration, and one is ultra-high-definition (UHD) low-light image restoration. In addition, we evaluate the effectiveness of the various components of our method on the task of multi-task image restoration.

4.1. Multi-task Image Restoration

We conduct experiments across several standard low-level vision tasks, including single-image deraining, motion de-

blurring, defocus deblurring, and image denoising. All comparison methods were retrained on a small-scale dataset distilled from the Restormer [37].

Datasets. We employ the Rain100L [35], Rain100H [35], GoPro [19], RealBlur-J [27], RealBlur-R [27], DPDD [2], SIDD [1], and DND [24] datasets for benchmarking. These datasets provide a wide variety of image degradations, allowing us to evaluate the generalizability of TripleD across different tasks.

Training Setting. All models are trained using the AdamW optimizer, with an initial learning rate of 3×10^{-4} , and a cosine annealing learning rate scheduler is applied. Training is conducted on patches of size 384×384 , with a batch size of 16. In cases where the datasets are relatively small, we employ the TripleD strategy, dynamically selecting 2% of the data in each epoch. We conduct an experiments on a single NVIDIA RTX 3090 GPU for both TripleD and baseline single-GPU training, following the original setup of the Restormer. To comprehensively assess the effectiveness of our strategy, we use two widely adopted metrics: Peak Signal-to-Noise Ratio (PSNR) [13] and Structural Similarity Index Measure (SSIM) [33].

4.2. Baseline Comparisons

We summarize the quantitative performance of our TripleD method against the full-dataset training and single-GPU baselines in Table 1 and Figure 4. Across various datasets and tasks, TripleD consistently achieves close to 90~95% of the performance of full-dataset training, despite using only 2% of the data. Notably, TripleD significantly reduces memory and computational costs, allowing it to run efficiently on a single GPU. In the supplementary material, we show some real-world scenarios for our algorithm.

4.3. Experimental Analysis

In this section, we show some quantitative and qualitative analyses to explain the effectiveness of our method.

Diversity Analysis of Distilled Samples To quantitatively compare the diversity of distilled samples under GSDD and our TripleD strategy, we compute the pairwise Euclidean distances (PED) and pairwise feature distances (PFD) between feature embeddings (extracted by ResNet-50) of 200 distilled samples, and plot their cumulative distribution functions (CDFs). As shown in Figure 5, TripleD exhibits a right-shifted CDF in both metrics—indicating higher sample diversity, which helps the model generalize better under extreme pruning ratios.

Effectiveness of CNN. In the Rain100L deraining task, we experimented with different CNNs to evaluate their effectiveness. Specifically, we compare the performance of CNNs with different layers. Here, we do not consider the computationally expensive Transformer. Table 2 summa-

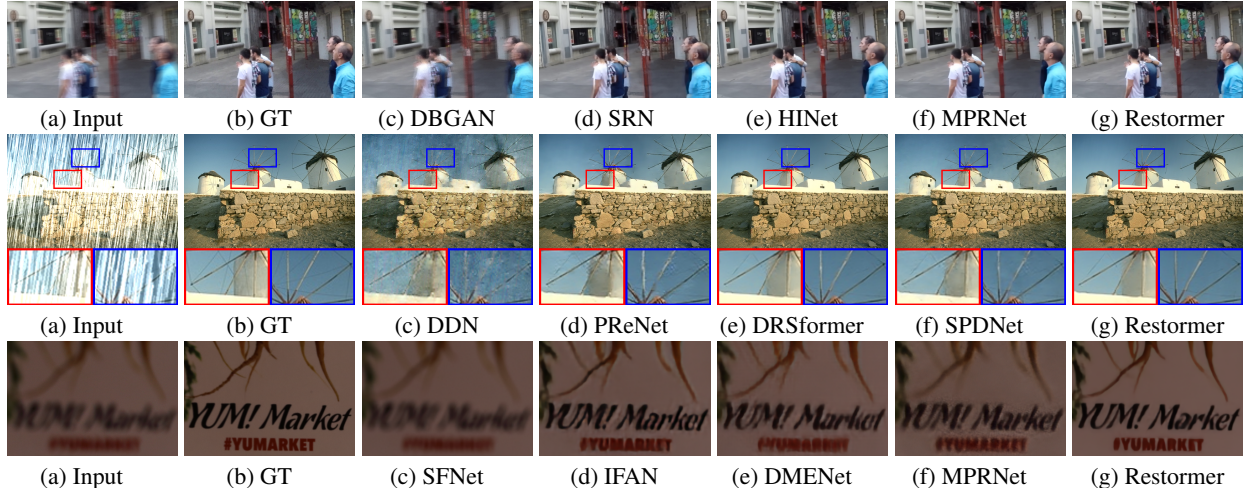


Figure 4. Visual comparisons with state-of-the-art methods on the GoPro, Rain100 and DPDD datasets. All comparison methods are retrained on the Restormer synthesised dataset.

Table 1. Performance comparison between Restormer (multi-GPU), our TripleD approach (Restormer is retrained on our synthetic dataset), and Restormer (single-GPU, large-resolution images are processed in chunks) across different image restoration tasks. PSNR/SSIM values are reported for each method, and tasks that cannot be trained on a single GPU are marked with a “-”.

Dataset	Task	Restormer (Multi-GPU)	Ours (Single-GPU)	Restormer (Single-GPU)
Rain100L [35]	Deraining	36.52 / 0.925	32.08 / 0.910	33.22 / 0.921
Rain100H [35]	Deraining	29.46 / 0.851	28.05 / 0.823	28.89 / 0.840
Test100 [39]	Deraining	30.12 / 0.867	28.25 / 0.830	29.01 / 0.849
Test1200 [39]	Deraining	32.46 / 0.899	30.78 / 0.875	31.11 / 0.876
GoPro [19]	Deblurring	30.25 / 0.935	29.12 / 0.889	26.50 / 0.880
RealBlur-J [27]	Real-world Deblurring	33.12 / 0.952	31.67 / 0.938	30.80 / 0.930
RealBlur-R [27]	Real-world Deblurring	33.12 / 0.952	31.67 / 0.938	30.70 / 0.931
DPDD [2]	Defocus Deblurring	25.98 / 0.811	24.21 / 0.802	23.90 / 0.790
SIDD [1]	Denoising	40.02 / 0.955	38.12 / 0.919	37.50 / 0.910
DND [24]	Denoising	40.03 / 0.956	38.56 / 0.932	35.99 / 0.925

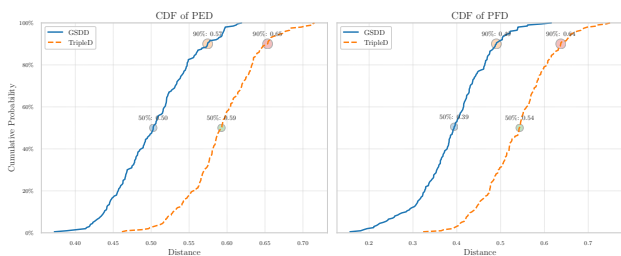


Figure 5. CDFs of pairwise distances between distilled-sample features under GSDD vs. TripleD. The left half shows PED and the right half shows PFD. In both metrics, the TripleD curves are right-shifted, indicating higher sample diversity.

rizes the results, where we report PSNR and SSIM for each CNN when applied in our framework.

Effectiveness of Downsampling. In the Rain100L deraining task, we experimented with different downsampling resolutions (64×64 , 384×384 , and full resolution) to evaluate

their effectiveness. Table 3 summarizes the results, where we report PSNR and SSIM for each downsampling resolution when applied in our framework. Figure 12 summarizes the distribution alignment achieved by different CNN adjustments, which visually demonstrates the improvements as the adjusted dataset more closely aligns with the target distribution in our framework.

Effectiveness of the proportion of synthetic dataset p . In the Rain100L deraining task, we experimented with different distillation hyperparameters p (1%, 5%, and 10%) to evaluate their effectiveness. Table 5 summarizes the results, where we report PSNR and SSIM for p when applied in our framework.

4.4. More Ablation Experiments

To further quantify the contribution of each module, we perform three additional ablation studies on the Rain100L deraining task. Table 6–Table 7 summarize the results.

Table 2. Performance of CNN. Only CNNs with 8 layers have good results, and it is not the case that the more convolutional layers the better.

Layers of CNN	PSNR (dB)	SSIM
0	30.33	0.897
4	31.12	0.889
16	32.05	0.908
Ours	32.08	0.910

Table 3. Performance of downsampling. Although full resolution performs better, it takes more than $50 \times$ longer.

Resolution of downsampling	PSNR (dB)	SSIM
64×64	27.11	0.844
Ours	32.08	0.910
384×384	31.89	0.911
Full resolution	33.21	0.912

Table 4. Performance of different feature extractors for dynamic sample selection on Rain100L deraining task.

Feature Extractor	PSNR (dB)	SSIM
ResNet-50	30.50	0.900
ViT	32.08	0.910
Mamba	31.10	0.879
MLP-Mixer	32.05	0.901

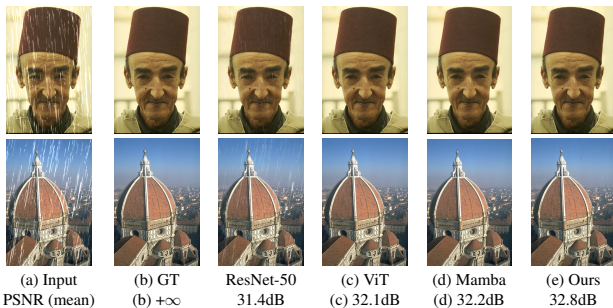


Figure 6. Visual comparison of rain removal results for two samples from the Rain100L dataset using various models: Input, Ground Truth (GT), ResNet-50, ViT, CLIP, and ViT+CLIP.

Table 5. Performance of p . To trade off accuracy and efficiency, we use 2% of the data size.

Distillation hyperparameter p	PSNR (dB)	SSIM
1%	25.33	0.831
Ours	32.08	0.910
5%	32.09	0.912
10%	33.14	0.925

Table 6. Effect of removing the CNN fine-tuning module on Rain100L deraining.

Configuration	PSNR (dB)	SSIM
Full TripleD (Ours)	32.08	0.910
w/o CNN Fine-Tuning	30.75	0.894

Table 7. Comparison of generative backbones for data distillation.

Backbone	PSNR (dB)	SSIM
SD3 Diffusion (Ours)	32.08	0.910
StyleGAN2	31.02	0.903

Table 8. Effect of Gradient Accumulation on PSNR, SSIM, and memory usage for deraining task. The use of gradient accumulation enables efficient training with reduced memory usage while maintaining competitive performance.

Accumulation Steps	Memory Usage (GB)	PSNR (dB)	SSIM
1 (No Accumulation)	24	32.15	0.922
4	17	32.08	0.910
8	12	31.91	0.900

4.5. Training Optimization

Due to the limited memory of a single NVIDIA RTX 3090 GPU (24GB), training large-scale models, such as Restormer, with full batch sizes is infeasible, especially when working with high-resolution images. To address this challenge, we employ gradient accumulation, which allows for the simulation of larger batch sizes without exceeding the memory limit by accumulating gradients over several mini-batches.

To demonstrate the efficacy of gradient accumulation, we conducted ablation studies across different accumulation steps (1, 4, and 8 steps) to evaluate its impact on memory usage, and restoration performance. Table 8 presents the results of this experiment. We observe that while memory usage significantly decreases as the accumulation steps increase, the impact on PSNR and SSIM is minimal, demonstrating the robustness of this technique.

4.6. Evaluation of the Feature Extractor

In the Rain100L deraining task, we experimented with different feature extractors to evaluate their effectiveness in computing sample complexity and uncertainty. Specifically, we compared ResNet-50 [11], Vision Transformer (ViT), MLP-Mixer and Mamba to understand their impact on dynamic sample selection. Table 4 summarizes the results, where we report PSNR and SSIM for each feature extractor when applied in our TripleD framework.

To visually demonstrate the effectiveness of different feature extractors in the Rain100L deraining task, we present qualitative comparisons of the results generated by

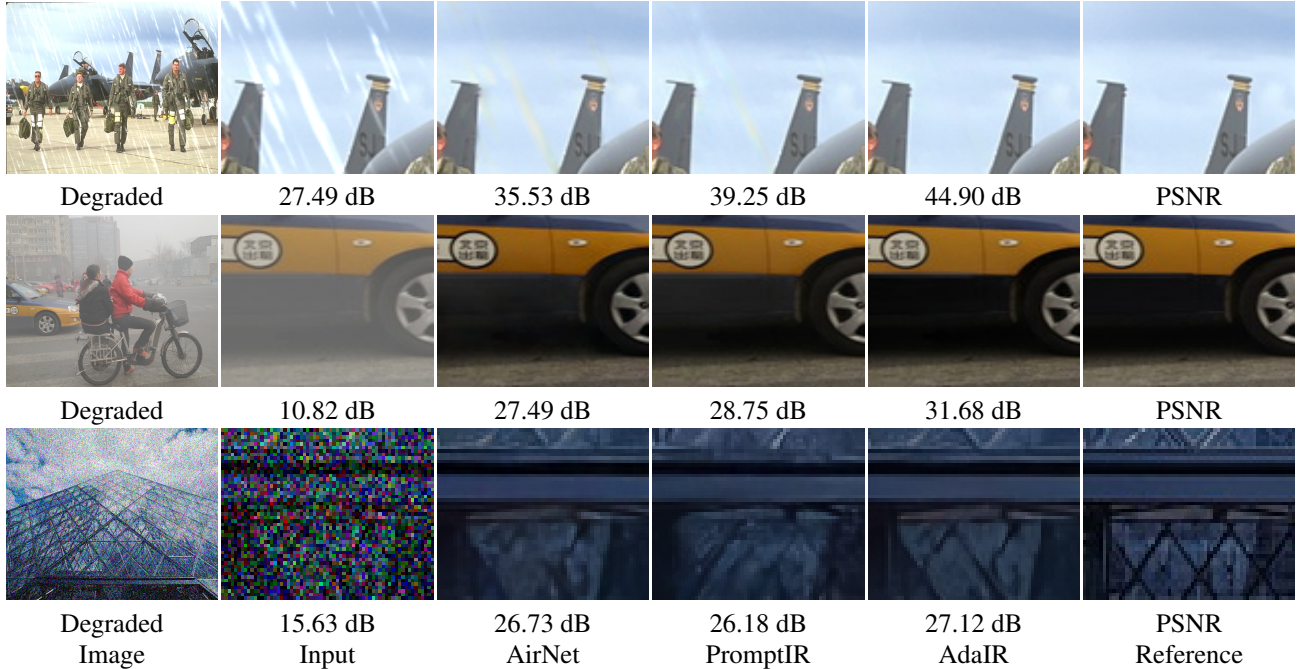


Figure 7. All-in-one model with TripleD. All comparison methods are retrained on the PromptIR synthesised dataset.

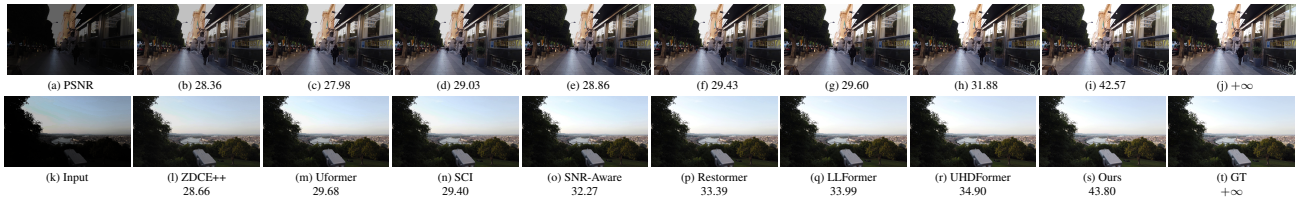


Figure 8. Comparison of methods on UHD-LOL4K dataset. All comparison methods are retrained on the UHDFormer synthesised dataset.

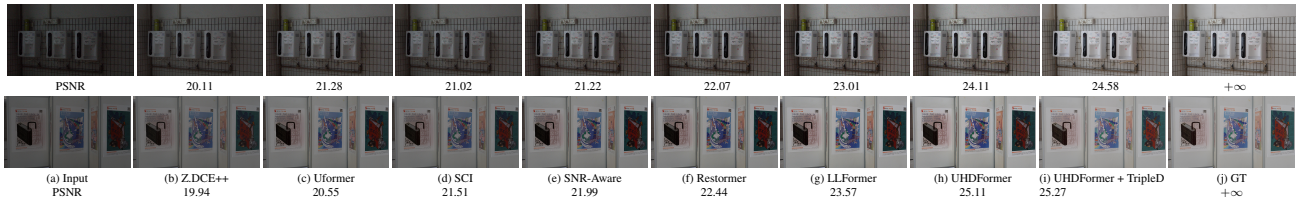


Figure 9. Comparison of methods on UHD-LL dataset. All comparison methods are retrained on the UHDFormer synthesised dataset.

Table 9. Performance comparison of PromptIR trained with TripleD against the pre-trained PromptIR model without TripleD.

Method	Dehazing on SOTS		Deraining on Rain100L		Denoising on BSD68 (PSNR/SSIM)		
	PSNR	SSIM	PSNR	SSIM	$\sigma = 15$	$\sigma = 25$	$\sigma = 50$
AirNet	34.90	0.968	27.94	0.962	33.92/0.933	31.26/0.888	28.00/0.797
AirNet with TripleD	32.11	0.923	26.86	0.912	32.12/0.913	30.57/0.826	27.90/0.779
PromptIR	30.58	0.974	36.37	0.972	33.98/0.933	31.31/0.888	28.06/0.799
PromptIR with TripleD	28.50	0.960	35.78	0.964	32.88/0.915	31.01/0.870	28.20/0.819
AdaIR	30.90	0.979	38.02	0.980	34.01/0.934	31.34/0.889	28.06/0.798
AdaIR with TripleD	30.49	0.971	35.08	0.968	33.88/0.909	31.00/0.877	28.15/0.809

ResNet-50, ViT, Mamba, and the MLP-Mixer combination. Figure 6 shows the input image and the corresponding derained outputs. MLP-Mixer and Mamba capture image

complexity in a relatively complementary relationship and are robust to degraded images. ViT shows a better restoration effect for TripleD. In the supplementary material, we

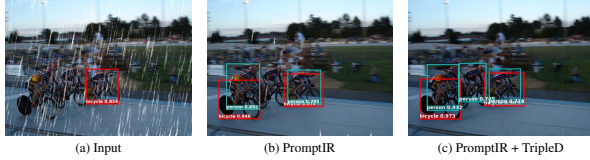


Figure 10. The qualitative results of object detection experiments on low-light transportation surveillance data, which select YOLOv5 [10] as the basic detection method.

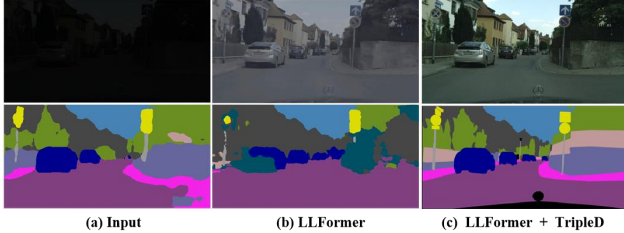


Figure 11. The results of segmentation experiments on the real world, which selects DAFormer [12] as the segmentation method.

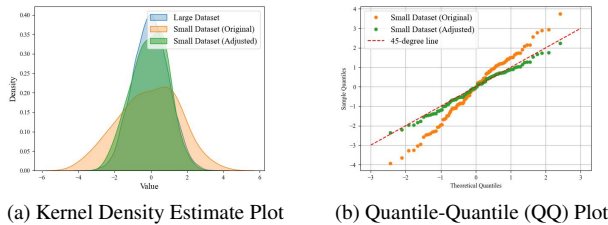


Figure 12. Distribution alignment visualization. (a) KDE plot shows that the adjusted small dataset distribution (green) aligns more closely with the large dataset distribution (blue), compared to the original small dataset (orange). (b) QQ plot illustrates the quantile alignment of the original (orange) and adjusted (green) small datasets with the theoretical quantiles of the large dataset.

have visualised some feature maps to illustrate their effectiveness.

4.7. Other Image Restoration Tasks

All-in-One Image Restoration. In this section, we evaluate the effectiveness of the TripleD method in training the well-known all-in-one model, PromptIR [25], across multiple degradation types. To ensure that each degradation type, such as rain, haze, and noise, is adequately represented during training, TripleD dynamically selects samples from each degradation category, balancing the number of samples chosen for each type. Table 9 shows the quantitative results in terms of PSNR and SSIM for different image restoration tasks, including dehazing on SOTS, deraining on Rain100L, and denoising on BSD68 with different noise levels ($\sigma = 15, 25, 50$). The PromptIR with TripleD achieved performance close to that of the re-trained PromptIR model, with some tasks showing slightly better performance. The hardware and parameter settings are the same as for multi-task image restoration. All comparison meth-



Figure 13. The qualitative results in the real world.

Table 10. Comparison of quantitative results on UHD-LOL4K.

Methods	Type	Venue	PSNR \uparrow	SSIM \uparrow
Z_DCE++ (TripleD)	non-UHD	TPAMI'21	15.58	0.934
Uformer (TripleD)		CVPR'22	29.98	0.980
Restormer (TripleD)		CVPR'22	36.90	0.988
NSEN (TripleD)	UHD	MM'23	29.49	0.980
UHDFour (TripleD)		ICLR'23	36.12	0.990
LLFormer (TripleD)		AAAI'23	37.33	0.988
UHDFormer		AAAI'24	36.28	0.989
UHDFormer (TripleD)		-	35.01	0.978

Table 11. Comparison of quantitative results on UHD-LL dataset.

Methods	Type	Venue	PSNR	SSIM
Z_DCE++ (TripleD)	non-UHD	TPAMI'21	16.41	0.630
Uformer (TripleD)		CVPR'22	19.28	0.849
SCI (TripleD)		CVPR'22	16.05	0.625
SNR-Aware (TripleD)		CVPR'22	22.17	0.866
Restormer (TripleD)		CVPR'22	22.25	0.871
LLFormer (TripleD)	UHD	AAAI'23	22.79	0.853
UHDFormer		AAAI'24	26.22	0.900
UHDFormer (TripleD)		-	24.95	0.869

ods were retrained on a small-scale dataset distilled from the PromptIR. As shown in Figure 7, we show the effectiveness of our method. As shown in Figure 10, we demonstrate an object detection task to show the effectiveness of our method.

UHD Image Restoration. In this section, we evaluate the effectiveness of the TripleD method in training the well-known UHD model, UHDFormer [15], across multiple low-light degradations. All comparison methods were retrained on a small-scale dataset distilled from the UHDFormer. Table 10 and 11 show the quantitative results in terms of PSNR and SSIM for low-light image restoration tasks. The UHDFormer with TripleD achieved performance close to that of the re-trained UHDFormer model, with some tasks showing slightly better performance. As shown in Figure 11, we demonstrate the effectiveness of our method by showing a semantic segmentation task. As shown in Figure 9 and 8, we show the effectiveness of our method. In the supplementary material, we show more results of UHD image enhancement, including defog, derain, and desnow.

5. Discussion and Conclusion

We observe that the CNN fine-tuned data set has a distribution that is closer to the distilled data set, as shown in

Figure 12. In addition, as shown in Figure 13, we demonstrate that our method has good generalisation in the real world. Additionally, there is an unsolved problem: why not directly use clear images (GT) for entropy evaluation? We found that using the dataset after image restoration is more robust for evaluation.

We address an important problem in image restoration, the training cost of the model. Our method uses only 2% of the image set to maintain 90% of the ability of the model trained on large-scale datasets. Especially for UHD image restoration tasks, we increase efficiency by more than 100 \times is trained on synthetic datasets. Extensive experimental results demonstrate the effectiveness of our methods.

References

- [1] Abdelrahman Abdelhamed, Stephen Lin, and Michael S Brown. A high-quality denoising dataset for smartphone cameras. In *CVPR*, 2018. 4, 5
- [2] Abdullah Abuolaim and Michael S Brown. Defocus deblurring using dual-pixel data. In *ECCV*, 2020. 4, 5
- [3] Eden Belouadah and Adrian Popescu. Scail: Classifier weights scaling for class incremental learning. In *WACV*, pages 1266–1275, 2020. 2
- [4] George Cazenavette, Tongzhou Wang, Mason Morehead, Jonathan Park, Kuno Singh, Dilip Krishnan, Deva Ramanan, and Eli Shechtman. Dataset distillation by matching training trajectories. In *Proceedings of the IEEE/CVF Conference on Computer Vision and Pattern Recognition (CVPR)*, pages 7027–7036, 2022. 2
- [5] George Cazenavette, Tongzhou Wang, Antonio Torralba, Alexei A Efros, and Jun-Yan Zhu. Generalizing dataset distillation via deep generative prior. In *CVPR*, pages 3739–3748, 2023. 4
- [6] Hanqing Chen, Yunhe Wang, Tianlong Guo, et al. Pre-trained image processing transformer. In *Proceedings of the IEEE/CVF Conference on Computer Vision and Pattern Recognition (CVPR)*, pages 12299–12310, 2021. 2
- [7] Jun Chen and Thomas Pock. Trainable nonlinear reaction diffusion for image restoration. *IEEE Transactions on Pattern Analysis and Machine Intelligence*, 39:1172–1185, 2017. 1
- [8] Tobias Dietz, Brian B Moser, Tobias Nauen, Federico Raue, Stanislav Frolov, and Andreas Dengel. A study in dataset distillation for image super-resolution. *arXiv preprint arXiv:2502.03656*, 2025. 2
- [9] Alexey Dosovitskiy, Lucas Beyer, Alexander Kolesnikov, et al. An image is worth 16x16 words: Transformers for image recognition at scale. In *International Conference on Learning Representations (ICLR)*, 2021. 2
- [10] Zheng Ge, Songtao Liu, Feng Wang, Zeming Li, and Jian Sun. Yolox: Exceeding yolo series in 2021. *arXiv preprint arXiv:2107.08430*, 2021. 8
- [11] Kaiming He, Xiangyu Zhang, Shaoqing Ren, and Jian Sun. Deep residual learning for image recognition. *Proceedings of the IEEE Conference on Computer Vision and Pattern Recognition (CVPR)*, pages 770–778, 2016. 6
- [12] Lukas Hoyer, Dengxin Dai, and Luc Van Gool. Daformer: Improving network architectures and training strategies for domain-adaptive semantic segmentation. In *Proc. IEEE CVPR*, pages 9924–9935, 2022. 8
- [13] Quan Huynh Thu and Mohammad Ghanbari. Scope of validity of psnr in image/video quality assessment. *Electronics letters*, 44(13):800–801, 2008. 4
- [14] Orest Kupyn, Viktor Budzan, Taras Mykhailiuk, Dmitry Mishkin, and Jiří Matas. Deblurgan: Blind motion deblurring using conditional adversarial networks. In *Proceedings of the IEEE Conference on Computer Vision and Pattern Recognition (CVPR)*, pages 8183–8192, 2018. 1
- [15] Chongyi Li, Chun-Le Guo, Man Zhou, Zhixin Liang, Shangchen Zhou, Ruicheng Feng, and Chen Change Loy. Embedding fourier for ultra-high-definition low-light image

- enhancement. In *International Conference on Learning Representations (ICLR)*, 2023. 8
- [16] Jingyun Liang, Jiezhong Cao, Guolei Sun, Kai Zhang, Luc Van Gool, and Radu Timofte. Swinir: Image restoration using swin transformer. In *Proceedings of the IEEE International Conference on Computer Vision (ICCV)*, pages 1833–1844, 2021. 2
- [17] Han Liu, Xiaoyang Guo, and Wei Wang. Low-level vision and dynamic sampling for high-fidelity image restoration. *IEEE Transactions on Image Processing*, 30:1575–1586, 2021. 2
- [18] Ilya Loshchilov and Frank Hutter. Sgdr: Stochastic gradient descent with warm restarts. *arXiv preprint arXiv:1608.03983*, 2016. 2
- [19] Seungjun Nah, Tae Hyun Kim, and Kyoung Mu Lee. Deep multi-scale convolutional neural network for dynamic scene deblurring. In *CVPR*, 2017. 2, 4, 5
- [20] Dai Nguyen, Minfeng Li, et al. Ramit: Reciprocal attention mixing transformer for lightweight image restoration. In *Proceedings of the IEEE/CVF Conference on Computer Vision and Pattern Recognition (CVPR)*, 2023. 2
- [21] Tan M Nguyen, Thang D Bui, Richard E Turner, and Yarin Gal. Dataset distillation with infinite ensembles. In *Advances in Neural Information Processing Systems (NeurIPS)*, 2022. 2
- [22] German I Parisi, Ronald Kemker, Jose L Part, Christopher Kanan, and Stefan Wermter. Continual lifelong learning with neural networks: A review. *Neural Networks*, 113:54–71, 2019. 2
- [23] Taeho Park and Sunghyun Kim. Freqformer: Frequency-aware transformer for lightweight image super-resolution. In *Proceedings of the International Joint Conference on Artificial Intelligence (IJCAI)*, 2024. 2
- [24] Tobias Ploetz and Stefan Roth. Benchmarking denoising algorithms with real photographs. In *CVPR*, 2017. 4, 5
- [25] Vaishnav Potlapalli, Syed Waqas Zamir, Salman Khan, and Fahad Khan. Promptir: Prompting for all-in-one image restoration. In *Thirty-seventh Conference on Neural Information Processing Systems*, 2023. 8
- [26] Sylvestre-Alvise Rebuffi, Alexander Kolesnikov, Georg Sperl, and Christoph H Lampert. icarl: Incremental classifier and representation learning. In *CVPR*, pages 2001–2010, 2017. 2
- [27] Sunghyun Rim, Hyungseok Son, and Seungyong Lee. Realblur: A new dataset for realistic blur synthesis and deblurring. In *CVPR*, 2020. 4, 5
- [28] Ozan Sener and Silvio Savarese. Active learning for convolutional neural networks: A core-set approach. *International Conference on Learning Representations (ICLR)*, 2018. 2
- [29] Burr Settles. Active learning literature survey. *University of Wisconsin, Madison*, 52(55-66):11, 2009. 2
- [30] Burr Settles. Active learning literature survey. *University of Wisconsin, Madison, WI*, 52(55-66), p.11, 2010. 2
- [31] Jiajun Wang, Yiqiao Tang, and Feng Li. Adaptive data selection strategies for efficient deep learning. In *Proceedings of the IEEE Conference on Computer Vision and Pattern Recognition (CVPR)*, pages 2385–2394, 2022. 2
- [32] Rui Wang, Ankit Goyal, Mohit Bansal, María Rojas-Carulla, Jakub M Tomczak, and Adrian Weller. Dataset distillation via optimal transport. In *Proceedings of the 38th International Conference on Machine Learning (ICML)*, pages 11535–11545, 2021. 1, 2
- [33] Zhou Wang, Alan C Bovik, Hamid R Sheikh, and Eero P Simoncelli. Image quality assessment: from error visibility to structural similarity. *IEEE transactions on image processing*, 13(4):600–612, 2004. 4
- [34] Chen Yang, Jing Liu, Jie Xu, and Lei Wang. Dynamic dataset distillation with uncertainty estimation. In *Proceedings of the IEEE/CVF Conference on Computer Vision and Pattern Recognition (CVPR)*, 2023. 2
- [35] Wenhan Yang, Robby T Tan, Jiashi Feng, Zhuwen Liu, Zhiding Guo, and Shuicheng Yan. Deep joint rain detection and removal from a single image. In *CVPR*, 2017. 4, 5
- [36] Shaohua Yin, Xiaoyang Zhang, Jian Wu, and Jun Chen. Image restoration with deep learning: A review. *IEEE Transactions on Neural Networks and Learning Systems*, 32:1967–1985, 2020. 1
- [37] Syed Waqas Zamir, Aditya Arora, Salman Khan, Munawar Hayat, Fahad Shahbaz Khan, and Ming-Hsuan Yang. Restormer: Efficient transformer for high-resolution image restoration. In *Proceedings of the IEEE/CVF Conference on Computer Vision and Pattern Recognition (CVPR)*, pages 5728–5739, 2022. 2, 4
- [38] He Zhang and Vishal M Patel. Density-aware single image de-raining using a multi-stream dense network. In *Proceedings of the IEEE Conference on Computer Vision and Pattern Recognition (CVPR)*, pages 695–704, 2018. 2
- [39] He Zhang and Vishal M Patel. Image de-raining using a conditional generative adversarial network. In *IEEE Transactions on Circuits and Systems for Video Technology*, 2018. 5
- [40] Kai Zhang, Wangmeng Zuo, Yunjin Chen, Dongwei Meng, and Lei Zhang. Beyond a gaussian denoiser: Residual learning of deep cnn for image denoising. In *IEEE Transactions on Image Processing*, pages 3142–3155, 2017. 2
- [41] Kun Zhang, Wang Zuo, Yandong Chen, and Lei Zhang. Image deraining with feature attention. In *Proceedings of the IEEE International Conference on Computer Vision (ICCV)*, pages 50–58, 2019. 1
- [42] Lei Zhang, Wang Zuo, Yandong Chen, and Kun Zhang. Image restoration: A comprehensive review. In *IEEE Transactions on Pattern Analysis and Machine Intelligence*, 2021. 1
- [43] Bo Zhao and Hakan Bilen. Dataset condensation with gradient matching. In *Proceedings of the IEEE/CVF Conference on Computer Vision and Pattern Recognition (CVPR)*, pages 708–717, 2021. 2
- [44] Xin Zhao, Liu Yang, and Hao Zhou. Dataset distillation: A comprehensive review. *arXiv preprint arXiv:2301.04866*, 2023. 2